Composites: Part B 60 (2014) 111–118

Contents lists available at ScienceDirect

Composites: Part B

journal homepage: www.elsevier.com/locate/compositesb

Effect of ball milling on graphene reinforced Al6061 composite fabricated by semi-solid sintering

Mina Bastwros [a], Gap-Yong Kim [a,*], Can Zhu [a], Kun Zhang [b], Shiren Wang [b], Xiaoduan Tang [a], Xinwei Wang [a]

[a] Department of Mechanical Engineering, Iowa State University, Ames, IA 50011, USA
[b] Department of Industrial Engineering, Texas Tech University, Lubbock, TX 79409, USA

ARTICLE INFO

Article history:
Received 9 July 2013
Received in revised form 19 December 2013
Accepted 22 December 2013
Available online 31 December 2013

Keywords:
A. Metal–matrix composites (MMCs)
A. Particle-reinforcement
B. Microstructures
E. Sintering

ABSTRACT

A 1.0 wt.% graphene reinforced aluminum 6061 (Al6061) composite was synthesized to investigate the effects of graphene dispersion by ball milling technique. The Al6061 powder and graphene were ball milled at different milling times. The composites were then synthesized by hot compaction in the semi-solid regime of the Al6061. A three point bending test was performed to characterize the mechanical properties of the composite. The ball milled powder and the fracture surfaces of the composites were analyzed using the scanning electron microscopy. A maximum enhancement of 47% in flexural strength was observed when compared with the reference Al6061 processed at the same condition.

1. Introduction

Since the second half of the twentieth century, metal matrix composites (MMCs) have been considered as one of the important materials. They are favored with superior properties compared with unreinforced metals and potentially offer ways to provide materials of higher strength-to-weight ratio, lower thermal expansion coefficient, and higher resistance to thermal fatigue and creep [1,2]. MMCs have made their ways into various applications in aerospace, electronic packaging, and automotive industries [3,4]. Recently, MMCs reinforced with nano-elements have attracted the interest of many researchers [5–10]. Graphitic structured materials like carbon nanotubes (CNTs), graphite, and graphene have been among the more widely researched materials due to their exceptional mechanical [11], thermal [12,13], electrical properties [14], and tribological behavior [15,16]. Moreover, improved manufacturing techniques have made these materials more affordable [17–21].

Various studies can be found in which CNTs were used as a reinforcement medium with different base metals like copper [8,22,23], aluminum [5,6,15,19,20,24–26], and their alloys [17,18,21,27]. Although some studies report significant mechanical property enhancement, CNT reinforced MMCs face various challenges. The uniform dispersion of CNTs and wetting between the CNT and the metal have been among the major concerns. Various researchers have used mechanical alloying (ball milling) as an effective means to disperse the CNTs [19,24,28–32]. Wu and Kim et al. [21], Esawi et al. [24,25], and Wang et al. [33] have investigated the effects of the mechanical alloying time on the dispersion of CNTs in ball milling. Kim et al. has investigated the effects of milling time on the CNT structure, and it was reported that the length of CNTs shortened significantly with increasing milling time [21,34]. Graphene, being the basic structural element for the CNT, also has a great potential as a reinforcing material but with a different form factor. The graphene is favored by excellent mechanical properties and high electrical and thermal conductivities [33]. Not much research, however, has been found on synthesis of metal–graphene composites and on understanding of graphene dispersion on mechanical properties.

In this study, a semi-solid processing technique has been used to synthesize an aluminum alloy composite reinforced by few-layer graphene oxide that has been manufactured by the modified Brodie's method [35]. The aluminum–graphene composite was synthesized in the semi-solid state of the aluminum alloy by pressure-assisted sintering. The technique has given good results for the aluminum–CNT composite in earlier studies performed by the authors [21,34,36,37]. A mechanical milling process was used to disperse the graphene in the matrix phase and its influence on mechanical properties and microstructure has been investigated.

* Corresponding author. Tel.: +1 515 294 6938.
E-mail address: gykim@iastate.edu (G.-Y. Kim).

1359-8368/$ - see front matter © 2013 Elsevier Ltd. All rights reserved.
http://dx.doi.org/10.1016/j.compositesb.2013.12.043

2. Materials and methods

Graphite was expanded to exfoliate graphene according to the modified Brodie's method. First, 10 g of graphite, 160 ml of nitric acid, and 85 g of sodium chlorate were mixed at room temperature. The mixture was kept for 24 h under continuous stirring. Then it was washed with 5% hydrochloric acid and distilled water for four times. The intercalated graphite was achieved through sedimentation and finally was dried at 60 °C. With the aid of ultrasonication, the intercalated graphite was exfoliated to monolayer or "few-layer" graphene oxide [35].

Aluminum alloy 6061 (Al6061) was used as the matrix phase, and its chemical composition is listed in Table 1. Mechanical alloying was performed using a SPEX 8000x ball milling machine to disperse the graphene into the Al6061 particles. The initial average sizes of Al6061 and graphene particles were 13.8 μm and 100 μm, respectively.

Al6061–1.0 wt.% graphene samples were prepared at various ball milling times: 10, 30, 60, and 90 min. In addition, a reference sample was prepared for each ball milling time with only Al6061 powder to isolate the strain hardening effect that came from the ball milling. The ball milling was performed in ambient conditions without any process controlling agents. 0.05 g of graphene was mixed with 4.95 g of Al6061 in a zirconia vial. Two zirconia balls, weighing 7.5 g each, were used in the mixing process, resulting in a ball to powder ratio (BPR) of 2.6. The ball mill was stopped for 30 min after every 10 min of operation, to prevent heating of the powder.

The experimental setup used for the composite synthesis is shown in Fig. 1. The die was made of H13 tool steel and was lubricated by spraying a thin layer of boron nitride to prevent a potential reaction between the aluminum and the die at elevated temperatures. The consolidation was performed in two stages. First, a pre-compaction pressure of 50 MPa was applied to the alloyed powder at room temperature. Then, the powder compact was hot-pressed at 100 MPa for 10 min in the mushy zone (between the solidus and liquidus temperature of Al6061) at 630 °C. The liquid phase fraction at this temperature is about 18%.

The obtained composites were cut using a low-speed diamond saw and were polished to the final dimensions (0.9 mm in thickness and 1.2 mm in width) needed to perform a three-point bend test. The flexural stress and flexural strain were recorded using the materials testing system. The fracture surfaces and the ball milled powder were examined using a scanning electron microscope, or SEM (FEI Quanta-250 field-emission scanning electron microscope). An XRD analysis was performed to check the carbide formation during consolidation. A Raman spectroscopy analysis was performed to study the effect of mechanical milling on the evolution of the graphene structure. Raman spectra of graphene were obtained using a confocal Raman spectrometer (Voyage, B&W Tek, Inc.). The laser beam (λ = 532 nm) was focused using a 50× objective lens before irradiating the samples. The laser energy was 2 mW and was uniformly distributed in space; this did not damage the samples. The laser spot size was $2 \times 4\ \mu m^2$, and was determined by using a blade method.

Table 1
Chemical composition of Al6061.

Element	Cr	Cu	Fe	Mg	Mn	Si	Ti	Zn	Al
Amount (%)	0.09	0.28	0.27	1.03	0.03	0.52	0.01	0.06	Bal.

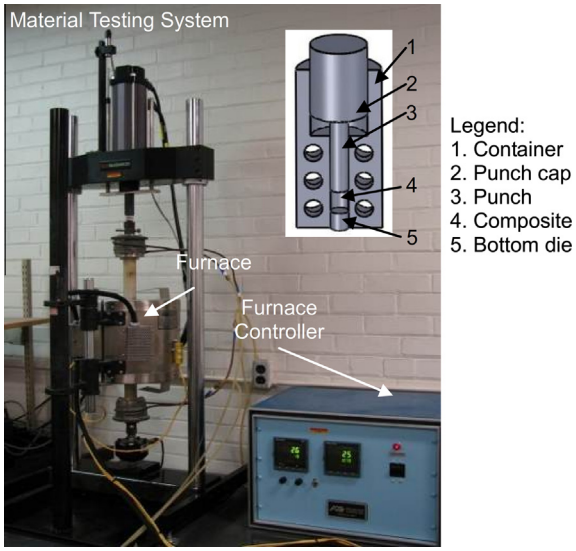

Fig. 1. Experimental setup for semi-solid sintering.

3. Results and discussion

With the aid of sonication, the intercalated graphite was exfoliated to few-layer graphene, while some of them were in the monolayer state. A transmission electron microscopy (TEM) image of few-layer graphene is shown in Fig. 2.

A portion of the mechanically alloyed powder was extracted at the specified milling times (30, 60, and 90 min) for analysis under the SEM. As shown in Fig. 3, the alloyed particle size increased with longer milling times. However, the graphene size decreased as the milling time increased. During mechanical alloying, cold welding and fracturing mechanisms compete with each other. Cold welding is dominant for the ductile Al6061 particles as they strain harden by the impact from the balls [24,34]. On the other hand, the agglomerated graphene is fractured and delaminated. These fractured graphene flakes are repeatedly enclosed and embedded into the cold welded aluminum particles by ball milling. Comparing the alloyed powder at 30 min and again at 60 min in Fig. 3, the overall particle size increased while the graphene flakes decreased in size. At 90 min, it was noticed that the composite particle shape had changed from platelet to particulate shape. It was also very difficult to locate the graphene, which indicated that the majority of the graphene had been embedded into the aluminum particles by ball milling process.

Raman spectroscopy was employed to check the evolution of graphene structure during composite processing. Three samples were used: (1) as-received graphene; (2) Al6061 alloyed with

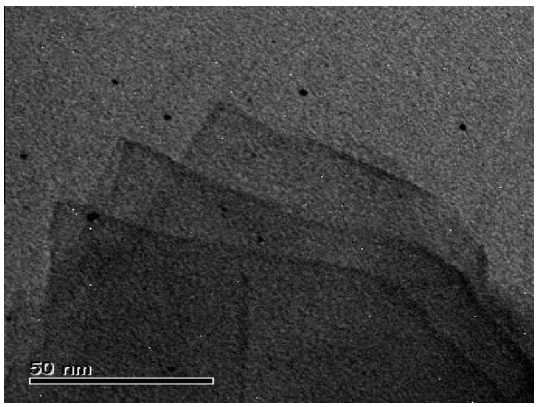

Fig. 2. TEM image of few-layers graphene.

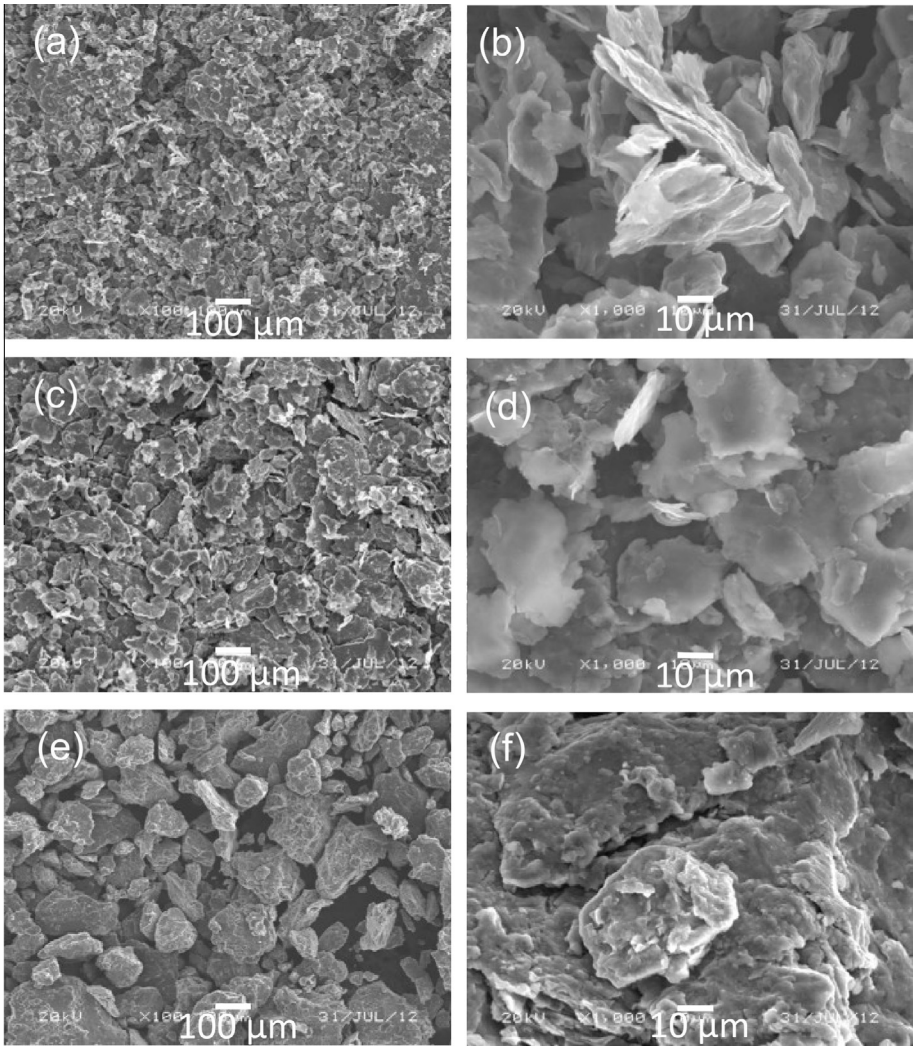

Fig. 3. SEM images of the milled Al6061-1.0 wt.% graphene powder at different milling times: (a and b) milled for 30 min, (c and d) milled for 60 min, (e and f) milled for 90 min.

2.0 wt.% graphene particles ball milled for 90 min; and (3) Al6061 alloyed with 2.0 wt.% graphene particles ball milled for 5 h. Samples with higher concentration of graphene (Al6061-2.0 wt.% graphene) were used to enhance the accuracy of the data collected during the Raman test. The higher the graphene concentration is, the higher the signal intensity is. 90 min of milling time was the maximum milling time used to synthesize the samples used in this study. Prolonged milling time, however, was needed to provide insight into the progression of damage in the graphitic structure beyond the milling times used to make the composites. Therefore, Raman measurement data for the 5 h of milling time sample were provided, which showed further changes in the graphitic structure that were not apparent. Fig. 4 shows the Raman spectra of graphene samples. The integration time was 60 s. The Raman peaks are fitted with the Lorentz function to obtain the precise Raman intensity and wavenumber. The results are summarized in Table 2.

The Raman spectrum of the as-received graphene oxide samples shows a D-band at 1349 cm^{-1}, a G-band at 1573 cm^{-1}, and a 2D-band at 2667 cm^{-1}. The G-band is the intrinsic vibration mode of a single graphite crystal. The D-band is related to the disorder in the graphene oxide and presence of sp^3 defects. The 2D-band is the overtone of the D-band, and is much smaller with respect to the D and G peaks.

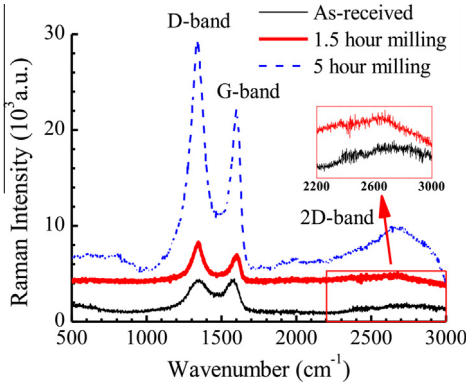

Fig. 4. Raman spectra of the milled Al6061-2.0 wt.% graphene powder at different milling times and as-received graphene.

The Raman spectra of graphene are related to the quality of the samples. The intensity ratio of D-band to G-band (I_D/I_G) indicates the disordering and defect density in the graphitic structures. After ball milling for 90 min, I_D/I_G increased from 1.1 to 1.4, which indicated disordering and defects in the graphene structure [38]. The

Table 2
Raman data of the milled Al6061-2.0 wt.% graphene particles.

State	I_D/I_G	I_G/I_{2D}	ω_G (cm^{-1})
As-received	1.08	0.65	1572.7
90 min milling	1.46	0.38	1593.9
5 h milling	1.42	0.28	1594.0

amount of defects increased in the graphene after the ball milling because of the physical force applied during the process. In Table 2, the ratio of the I_D/I_G increased to 1.46 after 90 min of ball milling, which indicated that the ball milling introduced more defects and disorder to the graphene clusters. After further milling up to 5 h, the I_D/I_G ratio did not change, which implied that there were no further defects introduced to the graphene structure. That could be attributed to the fact that the graphene sheets were embedded inside the Al6061 particles, which helped to protect them from further damage.

The ratio of integrated intensities I_G/I_{2D} decreases as the number of layers decrease [39]. The ratio of I_G/I_{2D} dropped from 0.65 to 0.38 after the sample was milled for 90 min. After further ball milling for up to 5 h, the ratio decreased to 0.28. The number of graphene layers changed from four layers to two (bilayer), and finally reached a monolayer configuration according to the reference [39]. The number of graphene layers dropped due to the physical force introduced in the powder composite during the mechanical alloying, which helped to separate the graphene layers from each other.

The peak position of the G-band (ω_G) indicates the stress experienced in the graphene. When graphene is strained, the interatomic distances of the graphene change; hence the vibration frequency of the G-band changes, which leads to a wavenumber shift. When the strain is larger, so is the shift of the wavenumber. In the experiments, the wavenumber increased from 1573 cm^{-1} (the as-received graphene) to 1594 cm^{-1} after 90 min of ball milling. The interatomic distances in the graphene were reduced, and the residual compressive stresses increased in the samples. The wavenumber, however, increased a small amount (~0.1) between a milling time of 90 min and 5 h of milling time, which indicated that the stress experienced by the graphene did not change significantly [40].

The flexural stress and strain were calculated from the measured force and displacement data using Eqs. (1) and (2) [34].

$$\sigma_{fl} = 3PL/2wh^2 \quad (1)$$

$$\varepsilon_{fl} = 6d_c h/L^2 \quad (2)$$

σ_{fl} and ε_{fl} are the flexural stress and flexural strain, respectively. P is the load; L is the support span; w and h are the width and depth of the specimen, respectively; and d_c is the deflection at the middle of the span.

The calculated flexural stress and strain curves of the Al6061-1.0 wt.% graphene composites are plotted in Fig. 5 along with the reference Al6061 milled for the same duration. In general, the strength of the graphene-reinforced composite and the reference Al6061 increased as the mechanical alloying time increased, while the flexural strain to failure decreased [41]. The strengthening in the reference Al6061 can be attributed to strain hardening by ball milling [42]. The strength increase in the graphene-reinforced composite may come from three main contributors: graphene addition [33]; strain hardening due to ball milling [6,21,24,26,34]; and carbide formation due to the reaction between the molten aluminum and defects at the graphitic planes [7]. By comparing the bend test results of the composite with the reference sample, strengthening due to strain hardening may be estimated.

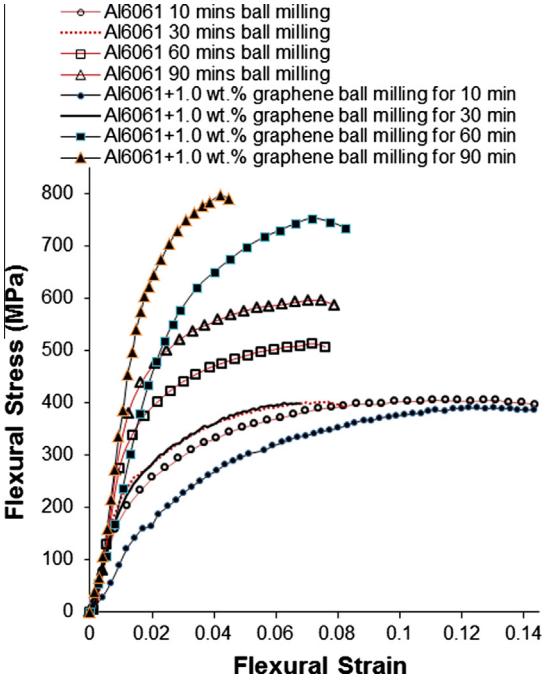

Fig. 5. Flexural stress–strain curves of Al6061-1.0 wt.% graphene.

In Fig. 5, the addition of graphene did not improve the strength for Al6061-1.0 wt.% graphene composites made at 10 min and 30 min milling times when compared with the reference Al6061 consolidated under the same conditions. The milling times were not long enough to fully disperse the graphene into the Al6061 matrix particles [24,34] resulting in degradation of mechanical properties. With only 10 min of milling, it was observed that the agglomeration of graphene significantly weakened the composite, to a point where the strength was less than the reference Al6061 (without any graphene). This conglomeration interrupts the consolidation and results in producing defects in the composite [43–45]. As the milling time increased to 60 min and 90 min, the flexural strengths increased significantly to 760 MPa and 800 MPa, respectively. Compared with the corresponding Al6061 reference sample (milled for the same milling time), the strength increase was 47% and 34% for the 60-min and 90-min composites, respectively. The strengthening may be due to the addition of 1.0 wt.% graphene and/or carbide that formed during the synthesis [21,34]. Unfortunately, the individual contributions from the graphene and the carbide cannot be evaluated at this point. Fig. 6 shows the XRD analysis results for the Al6061-1.0 wt.%

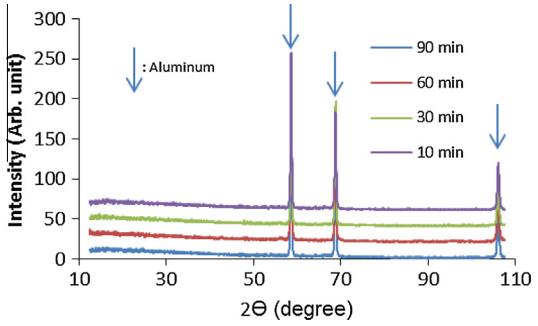

Fig. 6. XRD analysis of the Al6061-1.0 wt.% graphene samples at different milling times.

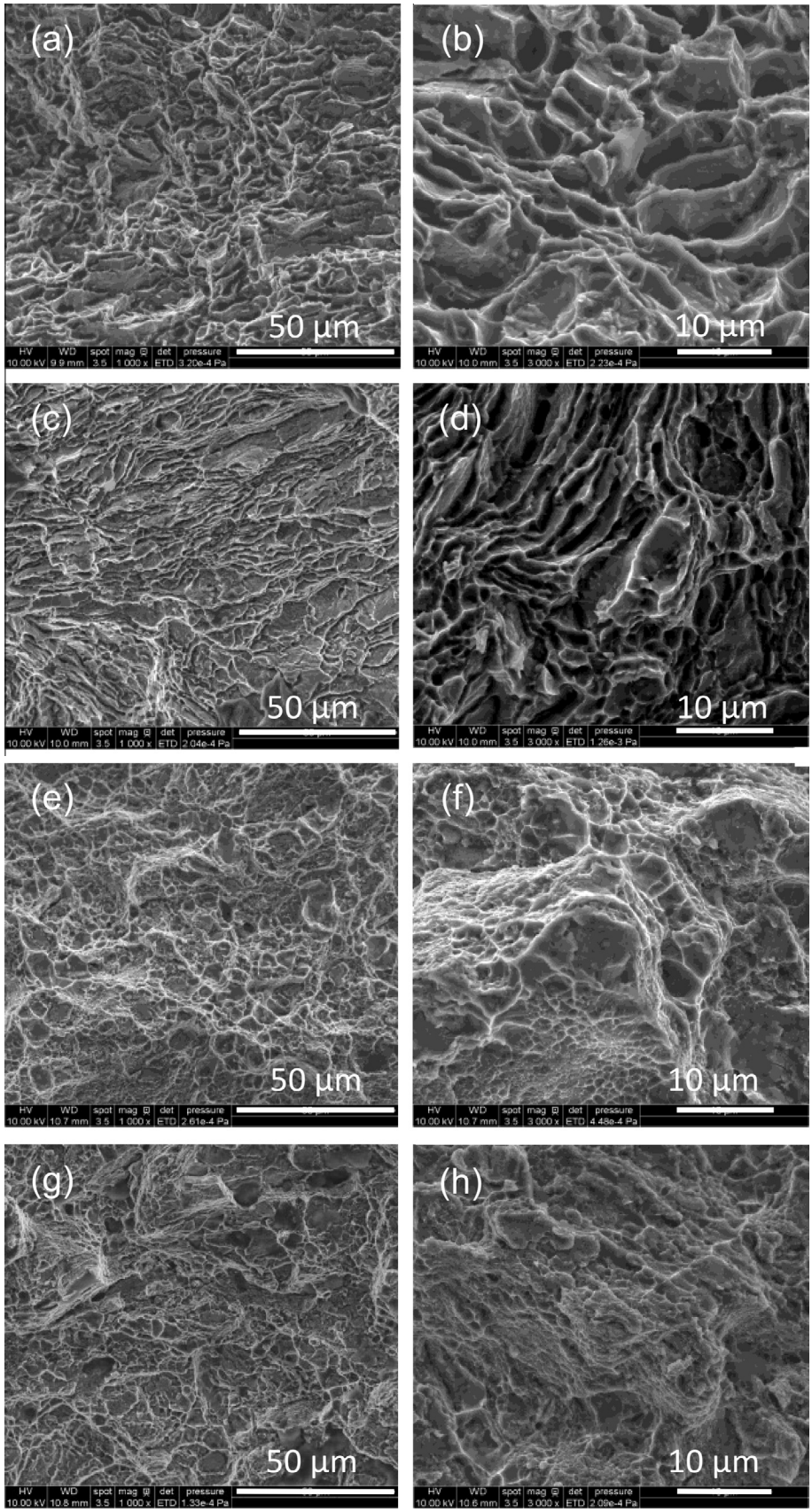

Fig. 7. SEM images of fracture surfaces of the Al6061-1.0 wt.% graphene composites prepared at different milling times: (a and b) 10 min, (c and d) 30 min, (e and f) 60 min, and (g and h) 90 min.

graphene samples at various milling times. Aluminum carbide peaks were not detected, but this does not necessarily mean that no carbide was formed. The amount of carbide formation may be below the level of sensitivity of the XRD apparatus used, which is about 1.0 wt.%.

In Fig. 7, SEM images of the fracture surfaces of the Al6061-1.0 wt.% graphene composites that were prepared at different milling times are presented. As shown in Fig. 7, the plastic deformation, represented by the ductile fracture dimples, decreased as milling time increased. Comparing the 30-min (Fig. 7 (c and d)) and the 60-min (Fig. 7 (e and f)) milling time samples, a change in the morphology of the surface is observed. The dimples of the ductile fracture observed in the 30-min sample diminished and numerous flat regions were detected on the 60-min sample fracture surface. As the milling time increased, the sharp decrease in the size of the ductile dimples of the fracture surface indicated that the ductility of the composite had decreased significantly [34]. This change in the fracture surface was also accompanied by a change in the mechanical behavior as discussed and shown in Fig. 5. As discussed earlier, 30 min of milling was not enough for the graphene to be uniformly dispersed throughout the Al6061 matrix, resulting in no enhancement in, or even deterioration of the mechanical properties [43].

Fig. 8 compares the fracture morphology of Al6061 (no graphene) and Al6061-1.0 wt.% graphene ball milled for 90 min. It is evident that the size of the ductile dimples decreased significantly when graphene was added and dispersed within the matrix through ball milling. This indicates that the ductility decrease of the Al6061-1.0 wt.% graphene composite was most likely due to graphene addition and its dispersion rather than solely from the hardening effect from milling.

Fig. 9 shows a crack on the fracture surface on the Al6061-graphene composite ball milled for 10 min. These large cracks were not visible on the fracture surfaces of other composites that were milled for more time (30, 60, and 90 min). They were formed due to the poor interface between the large graphene cluster and the matrix phase, which acted as a crack nucleation site. Under the bending load, these cracks propagated and grew, accounting for the inferior flexural strength of the Al6061-graphene sample when compared with the reference Al6061 sample. For longer milling times (30, 60, and 90 min), the dispersed graphene acted as bridges preventing and/or delaying micro-crack propagation paths [46].

An exhaustive search for graphene was performed on all fracture surfaces. It was very difficult, however, to locate graphene for the 30-, 60-, and 90-min milling time samples. For the 10 min milling time sample, clusters of graphene layers were observed on the fracture surface as shown in Fig. 10. Fig. 10(a and b) shows graphene cluster embedded into the matrix phase. In Fig. 10(a), a change in phase was observed between the clustered graphene and the matrix. Fig. 10(b) shows the topography of the graphene cluster. In Fig. 10(c–e), a graphene cluster attached to the surface can be observed. For the graphene observed in this image, it was

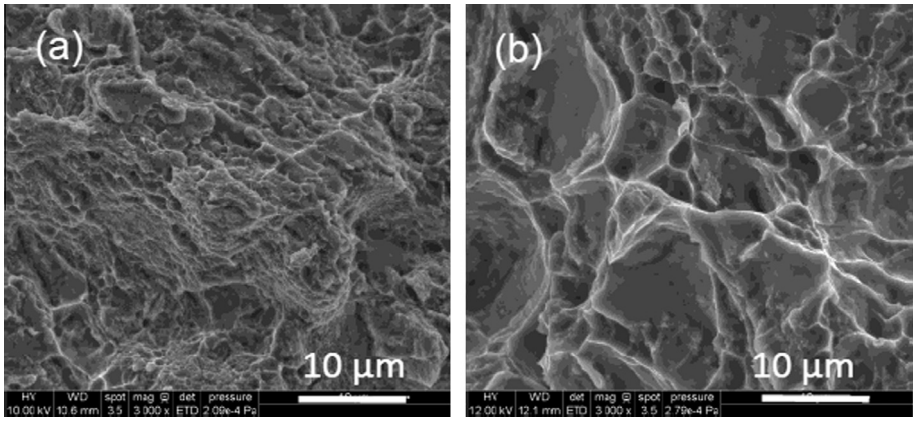

Fig. 8. SEM images of fracture surfaces: (a) Al6061-1.0 wt.% graphene milled for 90 min, and (b) Al6061 unalloyed milled for 90 min.

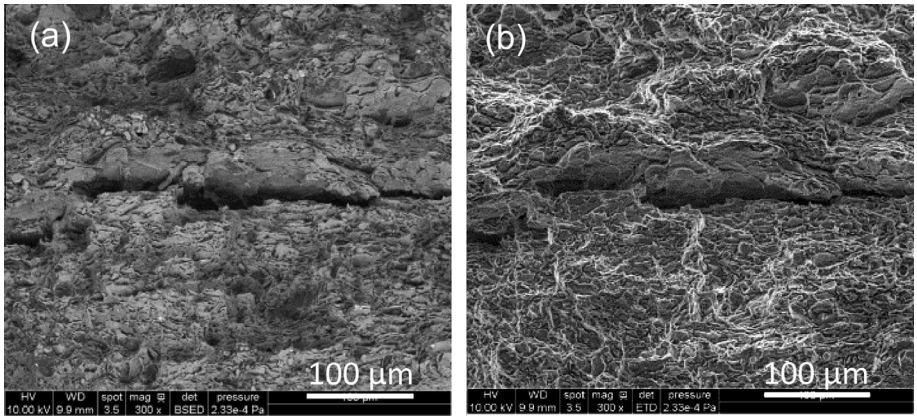

Fig. 9. SEM images of fracture surface of Al6061-1.0 wt.% graphene composite milled for 10 min showing a large crack that appeared on the surface: (a) BSEC detector, and (b) ETD detector.

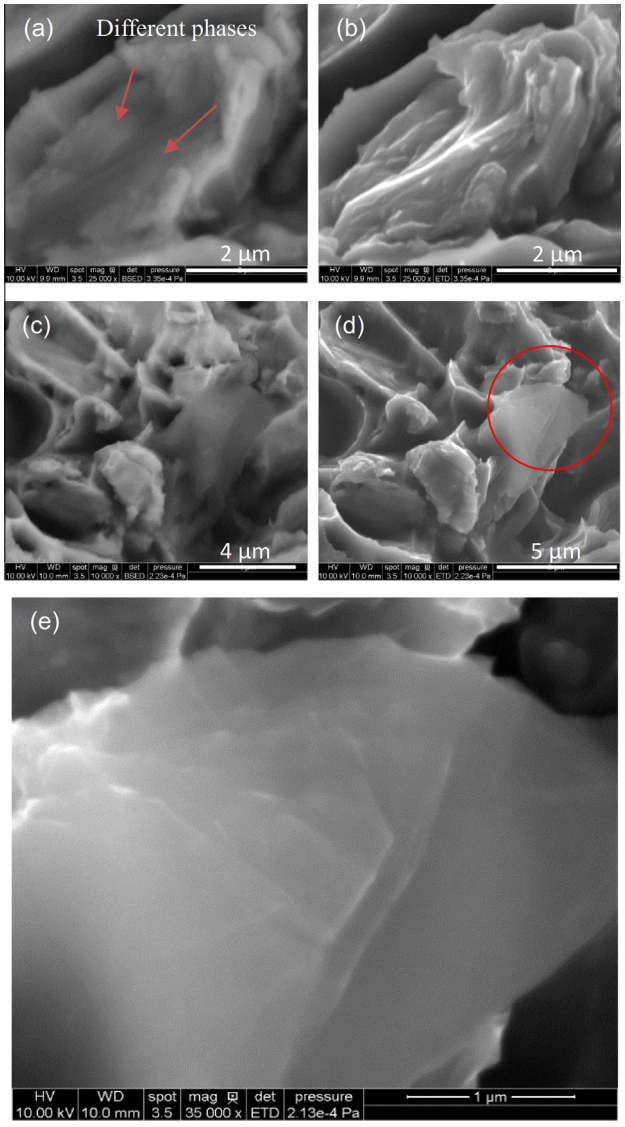

Fig. 10. Images of graphene clusters: (a) BSEC detector SEM image of a graphene cluster embedded in the Al6061 matrix, (b) ETD detector SEM image, (c) BSEC detector SEM image of a graphene cluster attached to the surface, (d) ETD detector SEM imaging, and (e) higher magnification of the graphene layers.

pulled normal to the fracture dimples in the direction of tensile loading caused by bend test. In Fig. 10(e), the layered graphene structure is clearly visible at high magnification.

4. Conclusions

In this study, the Al6061-1.0 wt.% graphene composites were fabricated by ball milling Al6061 particles and graphene, followed by pre-compaction at room temperature, and finally by hot compaction in the semi-solid regime. The ball milling time varied from 10 min to 90 min. The 10- and 30-min ball milling times were not enough to homogeneously disperse the graphene into the Al6061 matrix, which resulted in degradation of the flexural strength for the 10-min milling time sample and no enhancement for the 30-min milling time sample. The strength increase for the Al6061-1.0 wt.% graphene composite was 47% and 34% for the 60-min and 90-min times, compared with the reference Al6061 sample. According to the Raman analysis, further milling did not introduce more damage to the graphene, but instead helped to uniformly disperse the graphene and reduce the number of the stacked layers. It was concluded that the strengthening was significantly affected by the dispersion of the graphene in the matrix phase.

Acknowledgments

The authors greatly appreciate the financial support from the United States National Science Foundation (CMMI-1030120) and Defense Advanced Research Projects Agency (N66001-12-1-4257). Finally, the authors would like to thank the valuable discussions and support from Warren Straszheim, Michael Martin, and Jie Wang.

References

[1] Gasem ZM. Fatigue crack growth behavior in powder-metallurgy 6061 aluminum alloy reinforced with submicron Al2O3 particulates. Compos B Eng 2012;43(8):3020–5.
[2] Dyachkova L, Feldshtein EE. On the properties of composites based on sintered bronze with alumina additives. Compos B Eng 2013;45(1):239–47.
[3] Chawla N, Chawla KK. Metal matrix composites. Springer Science; 2006.
[4] Callistar W. Materials science and engineering. John Wiley & Sons; 2007.
[5] George R, Kashyap KT, Rahul R, Yamdagni S. Strengthening in carbon nanotube/aluminium (CNT/Al) composites. Scripta Mater 2005;53(10):1159–63.
[6] Esawi AMK, Morsi K, Sayed A, Taher M, Lanka S. Effect of carbon nanotube (CNT) content on the mechanical properties of CNT-reinforced aluminium composites. Compos Sci Technol 2010;70(16):2237–41.
[7] Bartolucci SF, Paras J, Rafiee MA, Rafiee J, Lee S, Kapoor D, et al. Graphene–aluminum nanocomposites. Mater Sci Eng A 2011;528(27):7933–7.
[8] Nam DH, Kim YK, Cha SI, Hong SH. Effect of CNTs on precipitation hardening behavior of CNT/Al–Cu composites. Carbon 2012;50(13):4809–14.
[9] Gopalakrishnan S, Murugan N. Production and wear characterisation of AA 6061 matrix titanium carbide particulate reinforced composite by enhanced stir casting method. Compos B Eng 2012;43(2):302–8.
[10] Baradeswaran A, Elaya Perumal A. Study on mechanical and wear properties of Al 7075/Al2O3/graphite hybrid composites. Compos B Eng 2014;56:464–71.
[11] Peng B, Locascio M, Zapol P, Li S, Mielke SL, Schatz GC, et al. Measurements of near-ultimate strength for multiwalled carbon nanotubes and irradiation-induced crosslinking improvements. Nat Nanotechnol 2008;3(10):626.
[12] Gardea F, Lagoudas DC. Characterization of electrical and thermal properties of carbon nanotube/epoxy composites. Compos Part B Eng 2014;56:611–20.
[13] Chen JK, Huang IS. Thermal properties of aluminum–graphite composites by powder metallurgy. Compos B Eng 2013;44(1):698–703.
[14] Balázsi C, Fényi B, Hegman N, Kövér Z, Wéber F, Vértesy Z, et al. Development of CNT/Si3N4 composites with improved mechanical and electrical properties. Compos B Eng 2006;37(6):418–24.
[15] Bastwros MMH, Esawi AMK, Wifi A. Friction and wear behavior of Al–CNT composites. Wear 2013;307(1–2):164–73.
[16] Baradeswaran A, Perumal AE. Wear and mechanical characteristics of Al 7075/graphite composites. Compos B Eng 2014;56:472–6.
[17] Pérez-Bustamante R, Pérez-Bustamante F, Estrada-Guel I, Licea-Jiménez L, Miki-Yoshida M, Martínez-Sánchez R. Effect of milling time and CNT concentration on hardness of CNT/Al2024 composites produced by mechanical alloying. Mater Charact 2013.
[18] Lim DK, Shibayanagi T, Gerlich AP. Synthesis of multi-walled CNT reinforced aluminium alloy composite via friction stir processing. Mater Sci Eng A 2009;507(1–2):194–9.
[19] Liao J, Tan M-J. Mixing of carbon nanotubes (CNTs) and aluminum powder for powder metallurgy use. Powder Technol 2011;208(1):42–8.
[20] Lahiri D, Bakshi SR, Keshri AK, Liu Y, Agarwal A. Dual strengthening mechanisms induced by carbon nanotubes in roll bonded aluminum composites. Mater Sci Eng A 2009;523(1–2):263–70.
[21] Wu Y, Kim G-Y. Carbon nanotube reinforced aluminum composite fabricated by semi-solid powder processing. J Mater Process Technol 2011;211(8):1341–7.
[22] Jang Y, Kim S, Lee S, Kim D, Um M. Fabrication of carbon nano-sized fiber reinforced copper composite using liquid infiltration process. Compos Sci Technol 2005;65(5):781–4.
[23] Cho S, Takagi K, Kwon H, Seo D, Ogawa K, Kikuchi K, et al. Multi-walled carbon nanotube-reinforced copper nanocomposite coating fabricated by low-pressure cold spray process. Surf Coat Technol 2012;206(16):3488–94.
[24] Esawi A, Morsi K. Dispersion of carbon nanotubes (CNTs) in aluminum powder. Compos A Appl Sci Manuf 2007;38(2):646–50.
[25] Esawi AMK, Morsi K, Sayed A, Taher M, Lanka S. The influence of carbon nanotube (CNT) morphology and diameter on the processing and properties of CNT-reinforced aluminium composites. Compos A Appl Sci Manuf 2011;42(3):234–43.
[26] Morsi K, Esawi AMK, Borah P, Lanka S, Sayed A, Taher M. Properties of single and dual matrix aluminum–carbon nanotube composites processed via spark plasma extrusion (SPE). Mater Sci Eng A 2010;527(21–22):5686–90.

[27] Lee SB, Matsunaga K, Ikuhara Y, Lee S-K. Effect of alloying elements on the interfacial bonding strength and electric conductivity of carbon nano-fiber reinforced Cu matrix composites. Mater Sci Eng A 2007;449–451:778–81.
[28] Darsono N, Yoon D-H, Kim J. Milling and dispersion of multi-walled carbon nanotubes in texanol. Appl Surf Sci 2008;254(11):3412–9.
[29] Munkhbayar B, Nine MJ, Jeoun J, Bat-Erdene M, Chung H, Jeong H. Influence of dry and wet ball milling on dispersion characteristics of the multi-walled carbon nanotubes in aqueous solution with and without surfactant. Powder Technol 2013;234:132–40.
[30] Liu ZY, Xu SJ, Xiao BL, Xue P, Wang WG, Ma ZY. Effect of ball-milling time on mechanical properties of carbon nanotubes reinforced aluminum matrix composites. Compos A Appl Sci Manuf 2012;43(12):2161–8.
[31] Wang L, Choi H, Myoung J-M, Lee W. Mechanical alloying of multi-walled carbon nanotubes and aluminium powders for the preparation of carbon/metal composites. Carbon 2009;47(15):3427–33.
[32] Choi HJ, Kwon GB, Lee GY, Bae DH. Reinforcement with carbon nanotubes in aluminum matrix composites. Scripta Mater 2008;59(3):360–3.
[33] Wang J, Li Z, Fan G, Pan H, Chen Z, Zhang D. Reinforcement with graphene nanosheets in aluminum matrix composites. Scripta Mater 2012;66(8):594–7.
[34] Wu Y, Kim G-Y, Russell AM. Effects of mechanical alloying on an Al6061–CNT composite fabricated by semi-solid powder processing. Mater Sci Eng A 2012;538:164–72.
[35] Wang S, Tambraparni M, Qiu J, Tipton J, Dean D. Thermal expansion of graphene composites. Macromolecules 2009;42(14):5251–5.
[36] Wu Y, Kim G-Y. Compaction behavior of Al6061 powder in the semi-solid state. Powder Technol 2011;214(2):252–8.
[37] Wu Y, Kim G-Y, Anderson IE, Lograsso TA. Fabrication of Al6061 composite with high SiC particle loading by semi-solid powder processing. Acta Mater 2010;58(13):4398–405.
[38] Ferrari AC, Robertson J. Interpretation of Raman spectra of disordered and amorphous carbon. Phys Rev B 2000;61(20):14095–107.
[39] Graf D, Molitor F, Ensslin K, Stampfer C, Jungen A, Hierold C, et al. Spatially resolved raman spectroscopy of single- and few-layer graphene. Nano Lett 2007;7(2):238–42.
[40] Mohiuddin TMG, Lombardo A, Nair RR, Bonetti A, Savini G, Jalil R, et al. Uniaxial strain in graphene by Raman spectroscopy: g peak splitting, Grüneisen parameters, and sample orientation. Phys Rev B 2009;79(20):205433.
[41] Esawi AMK, El Borady MA. Carbon nanotube-reinforced aluminium strips. Compos Sci Technol 2008;68(2):486–92.
[42] Suryanarayana C. Mechanical alloying and milling. Prog Mater Sci 2001;46(1–2):1–184.
[43] Kim I-Y, Lee J-H, Lee G-S, Baik S-H, Kim Y-J, Lee Y-Z. Friction and wear characteristics of the carbon nanotube–aluminum composites with different manufacturing conditions. Wear 2009;267(1–4):593–8.
[44] Jin-long J, Hai-zhong W, hua Y, Jin-cheng X. Fabrication and wear behavior of CNT/Al composites. Trans Nonfer Metals Soc China 2007;17(s1A):s113–6.
[45] Jun L, Ying L, Lixian L, Xuejuan Y. Mechanical properties and oil content of CNT reinforced porous CuSn oil bearings. Compos B Eng 2012;43(4):1681–6.
[46] Zhang J, Ju S, Jiang D, Peng H-X. Reducing dispersity of mechanical properties of carbon fiber/epoxy composites by introducing multi-walled carbon nanotubes. Compos B Eng 2013;54:371–6.